CHEMISTRY

Formation of hydrogen trioxide (HOOOH) in extraterrestrial ice analogs and its role as an oxidizer in prebiotic chemistry

Xilin Bai[1]†, Chunxiao Li[1]†, Yuheng Luo[2]†, Qi'ang Gong[1], Jinghui Lu[3], Jiuzhong Yang[3], Yang Pan[3], Zhenrong Sun[1], André K. Eckhardt[4]*, Rui Sun[2]*, Ralf I. Kaiser[2]*, Tao Yang[1]*

The formation and characterization of hydrogen trioxide have fascinated scientists for more than a century, due to its role as a prototype model for oxygen-chain bonding and as a key transient in antibody-catalyzed oxidation reactions relevant to the origin of life. However, the abiotic formation pathways to hydrogen trioxide have remained elusive. Here, we demonstrate in laboratory simulation experiments that hydrogen trioxide effectively forms in water–molecular oxygen ice analogs at temperatures as low as 5 kelvin under exposure to proxies of galactic cosmic rays. Exploiting synchrotron vacuum ultraviolet photoionization reflectron time-of-flight mass spectrometry, hydrogen trioxide along with hydrogen peroxide and the hydroperoxyl radical was identified during the temperature-programmed desorption of the irradiated ices. This abiotic synthesis expands the oxidant inventory on interstellar grains, icy moons, and Kuiper belt objects, offering a plausible source of essential oxidizers for prebiotic chemistry in space.

INTRODUCTION

Hydrogen trioxide (HOOOH)—the simplest polyoxide—has long been regarded as a key intermediate in atmospheric (*1*, *2*), biological (*3*, *4*), and environmental processes (*1*, *5*) since its initial proposal by Berthelot (*6*) in 1880. Extensive investigation of its preparation, reactivity, structural characterization, and quantum chemical properties began only in the 1960s (*7*). Czapski and Bielski (*8*) first claimed the production of HOOOH in the pulse radiolysis of acidified air-saturated aqueous solutions, followed by the ultraviolet (UV) absorption spectroscopy of HOOOH in the pulse radiolysis of air-saturated perchloric acid solution (*9*, *10*). Giguère *et al.* (*11*, *12*) identified the fundamental skeletal vibrations of HOOOH via infrared and Raman spectra exploiting electrically discharged mixtures of water (H_2O), hydrogen peroxide (HOOH), and oxygen (O_2) at cryogenic temperatures. Plesničar *et al.* (*13*–*16*) prepared HOOOH at low temperatures in organic solvents via ozonation of 1,2-diphenylhydrazines or through decomposition of hydrotrioxides (ROOOH) with R being an organic group.

Enlightened by the microscopic reversibility that HOOOH can be reductively generated from ozone (O_3) decomposition catalyzed by water (*17*), Wentworth *et al.* (*3*, *18*) suggested that antibodies adopt water as an electron source to catalyze its addition to singlet molecular oxygen ($^1O_2$), yielding HOOOH as a reactive intermediate. Engdahl and Nelander (*19*) characterized the fundamental vibrations of HOOOH in argon matrices, identifying its antisymmetric O—O stretch at 776 cm^{-1} as an ideal marker distinct from strong water absorption. Xu and Goddard *et al.* (*1*, *20*) theoretically delineated plausible mechanisms for HOOOH in a water-catalyzed reaction of water with $^1O_2$ or via decomposition of [$(HO_2)(HO_3)$] hydrogen-bonded complexes. Suma *et al.* (*21*) reported the first pure rotational spectra and precise geometrical structure of *trans*-HOOOH. High-level ab initio studies including the benchmark CCSD(T)-F12 calculations by Hollman and Schaefer (*22*) confirmed a zigzag skew-chain helical-type structure of *trans*-HOOOH with C_2 symmetry.

Despite the astrochemical and astrobiological importance of HOOOH in the interstellar medium and the Solar System, its formation mechanism under extraterrestrial-like conditions has remained poorly understood. Water ice—a potential precursor to HOOOH—is found ubiquitously in cold molecular clouds (*23*, *24*) and throughout the Solar System including Kuiper belt objects (*25*, *26*), comets (*27*, *28*), and icy moons such as Europa, Ganymede, and Callisto (*29*, *30*). Molecular oxygen—a critical molecular building block of HOOOH—has been detected in molecular clouds, e.g., Orion (*31*) and ρ Ophiuchi (Oph) A (*32*), and the condensed phase on the Galilean and Saturnian moons (*33*, *34*). Notably, molecular oxygen also exhibits high abundances in the coma of comet 67P/Churyumov-Gerasimenko (*35*).

The coexistence of H_2O and O_2 in interstellar and Solar System ices suggests that HOOOH could form via nonequilibrium processes such as through the interaction of H_2O-O_2 ices with ionizing radiation such as galactic cosmic rays (GCRs) or electrons trapped in the magnetospheres of the giant planets. However, experimental studies on irradiated H_2O-O_2 ices are limited. Under conditions simulating the icy Galilean moons, Cooper, Moore, and Hudson detected HOOH in proton irradiated H_2O and H_2O-O_2 ices (*36*) along with the hydroperoxyl (HOO) and hydrotrioxyl (HOOO) radicals (*37*, *38*). Zheng *et al.* (*39*) conducted electron irradiation studies of $H_2{}^{18}O$-O_2 ices and tentatively assigned the formation of HOOOH via a single HOO bending mode at 1350 cm^{-1}. However, the symmetric/antisymmetric HOO bending modes of HOOOH at 1347 and 1359 cm^{-1} overlap strongly with water absorption bands, thus complicating unambiguous identification (*19*). Consequently, conclusive evidence for the formation and identification of HOOOH in simulated extraterrestrial environments still remains elusive.

In this study, we present persuasive evidence on the formation and identification of HOOOH, alongside HOO, HOOH, and O_3 in low-temperature H_2O-O_2 ice analogs exposed to proxies of GCRs.

[1]State Key Laboratory of Precision Spectroscopy, East China Normal University, Shanghai 200062, P. R. China. [2]Department of Chemistry, University of Hawaii at Manoa, Honolulu, HI 96822, USA. [3]National Synchrotron Radiation Laboratory, University of Science and Technology of China, Hefei, Anhui 230029, P. R. China. [4]Lehrstuhl für Organische Chemie II, Ruhr-Universität Bochum, Bochum 44801, Germany.
*Corresponding author. Email: tyang@lps.ecnu.edu.cn (T.Y.); ralfk@hawaii.edu (R.I.K.); ruisun@hawaii.edu (R.S.); andre.eckhardt@ruhr-uni-bochum.de (A.K.E.)
†These authors contributed equally to this work.

By exploiting the temperature-programmed desorption (TPD) technique, we investigate the subliming products formed in the irradiated ices via the synchrotron vacuum UV photoionization reflectron time-of-flight mass spectrometry (SVUV-PI-ReTOF-MS) (*40*–*42*). We achieve unambiguous identification of HOOOH plus other key oxidants through photoionization efficiency (PIE) curve fitting, in conjunction with high-level quantum chemical calculations, quadrupole mass spectrometry, and isotopic labeling experiments. Our results demonstrate that HOOOH can form effectively on icy grains and surfaces of Galilean and Saturnian moons and comet 67P/Churyumov-Gerasimenko. These findings expand the molecular inventory of oxidants in space and enhance our understanding of their roles as key chemical sources to oxidize complex organics or even fuel extraterrestrial life in the outer Solar System. Our work may also motivate astronomical searches for HOOOH in star-forming regions and on the icy moons of Jupiter and Saturn, where HOOH has already been identified.

RESULTS

Computations

The SVUV-PI-ReTOF-MS method represents a unique technique to identify subliming species in the TPD phase based on the mass-to-charge ratio (*m*/*z*) of the ions and the adiabatic ionization energies (IEs) of the neutrals (*40*, *41*). Because experimental IEs of H_2O_3 isomers are unknown, we theoretically determined their adiabatic IEs at a level of sufficient accuracy (0.01 to 0.08 eV) (*43*). Our computations revealed two structural isomers, with geometries calculated at the CCSD(T)/aug-cc-pVTZ level of theory and adiabatic IEs and relative energies computed at the CCSD(T)/CBS//B3LYP/aug-cc-pVTZ level of theory (Fig. 1 and tables S1 to S3). Two conformers of HOOOH were located: *trans*-HOOOH (C_2 symmetry) and *cis*-HOOOH (C_s symmetry); these conformers differ only by 9 kJ mol^{-1} and are interconvertible via a low *cis*-*trans* isomerization barrier of only 22 kJ mol^{-1} (*5*, *44*, *45*). The hyperconjugative interaction between the lone pair of electrons at the oxygen atoms and the σ* orbital of the adjacent O—H bond optimizes the dihedral angle, thus achieving maximum stability and electron delocalization. Specifically, the dihedral angle for *trans*-HOOOH is 81.3°, whereas the corresponding angle for HOOH is 112° (*5*). This hyperconjugation effect also shortens the O—O bond length in *trans*-HOOOH to 143.5 pm, in contrast to the typical O—O bond length of 145.6 pm in HOOH. We also identified the water-oxygen molecular complex [O(H_2O)O] isomer that is less stable by 485 kJ mol^{-1} compared to *trans*-HOOOH. This C_{2v} symmetric isomer holds a central oxygen atom with a sp^3 hybridization, resulting in one unpaired electron on each of the terminal oxygen atoms. The adiabatic IEs of the aforementioned isomers were computed respectively to be 11.00 to 11.07 eV (*trans*-HOOOH), 10.90 to 10.97 eV (*cis*-HOOOH), and 11.09 to 11.16 eV [O(H_2O)O] (*5*, *45*).

Mass spectrometry

In the TPD phase of irradiated H_2O-O_2 ices, ion signals were observed at *m*/*z* of 32, 33, 34, and 50 at photon energies of 12.20 eV (Figs. 2 and 3, A to B). Because the products only contain hydrogen and oxygen atoms, we can link them to the molecular formulas of O_2 (32 u), HO_2 (33 u), H_2O_2 (34 u), and H_2O_3 (50 u), respectively. The blank experiment, which was conducted without exposing the ices to ionizing radiation, reveals only signal at *m*/*z* of 32 (O_2^+), i.e., the ionized molecular oxygen reactant, suggesting that HO_2, H_2O_2, and H_2O_3 are the result of the radiation exposure of the H_2O-O_2 ices.

Isotopic labeling experiments involving the $H_2{}^{18}O$-O_2 ices provided additional evidence on the formation of isotopically substituted products (Fig. 3, C and D, and figs. S1 and S2). For clarity, we distinguish the oxygen atoms in the reactants and products as ^{16}O and ^{18}O, respectively. Here, TPD profiles at *m*/*z* of 50, 52, 54, and 56 in the $H_2{}^{18}O$-$^{16}O_2$ ice at the photon energy of 12.20 eV can be respectively assigned to ion signals of $H_2{}^{16}O_3$, $H_2{}^{18}O^{16}O_2$, $H_2{}^{18}O_2{}^{16}O$, and $H_2{}^{18}O_3$, which yield a branching ratio of 1:1.25:1.03:1.13 after the integration of each TPD profile at distinct *m*/*z*. Similarly, TPD profiles at *m*/*z* of 33, 35, and 37 at the photon energy of 11.40 eV correspond to ions of $H^{16}O_2$, $H^{16}O^{18}O$, and $H^{18}O_2$ whose branching ratio is 1:0.74:1.07, while those at *m*/*z* of 34, 36, and 38 at the photon energy of 11.40 eV correspond to ions of $H_2{}^{16}O_2$, $H_2{}^{16}O^{18}O$, and $H_2{}^{18}O_2$ whose branching ratio is 1:1.24:0.90.

We also analyzed the subliming molecules via an electron-impact quadrupole mass spectrometer (EI-QMS) operating with 70-eV electrons. Here, ion signals were detected at *m*/*z* of 34 and 48 in the $H_2{}^{16}O$-$^{16}O_2$ ices, indicating the formation of $H_2{}^{16}O_2$ and $^{16}O_3$ (fig. S3). We cannot assign ion signals at *m*/*z* of 33 to $H^{16}O_2{}^+$ due to strong mass interference of $^{16}O_2{}^+$. The absence of signals at *m*/*z* of 50 ($H_2{}^{16}O_3{}^+$) can be attributed to low ion counts and limited sensitivity of EI-QMS. In the irradiated $H_2{}^{18}O$-$^{16}O_2$ ices, we may assign ion signals at *m*/*z* of 34, 36, and 38 as $H_2{}^{16}O_2{}^+$/$^{16}O^{18}O^+$, $H_2{}^{16}O^{18}O^+$/$^{18}O_2{}^+$, and $H_2{}^{18}O_2{}^+$, respectively (fig. S4). Ion signals at *m*/*z* of 33, 35, and 37 can originate from either mass interference or fragmentation of neighboring ions. We detected ions at *m*/*z* of 48, implying preferential formation of $^{16}O_3$ over other O_3 isotopologues (*39*). Similarly, we did not observe any H_2O_3 isotopologues via EI-QMS in the irradiated $H_2{}^{18}O$-$^{16}O_2$ ices.

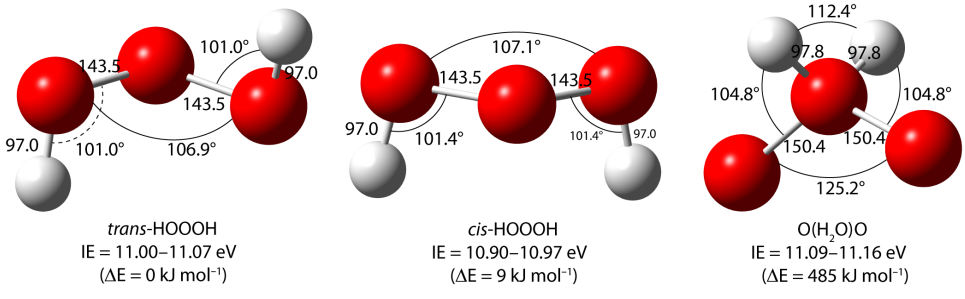

Fig. 1. CCSD(T)/aug-cc-pVTZ optimized geometries of H_2O_3 isomers. Bond lengths and angles are in the units of picometers (pm) and degrees (°), respectively, while relative energies with respect to *trans*-HOOOH (ΔE) are given in the units of kilojoules per mole (kJ mol^{-1}). Corresponding adiabatic IEs are provided in electron volts (eV).

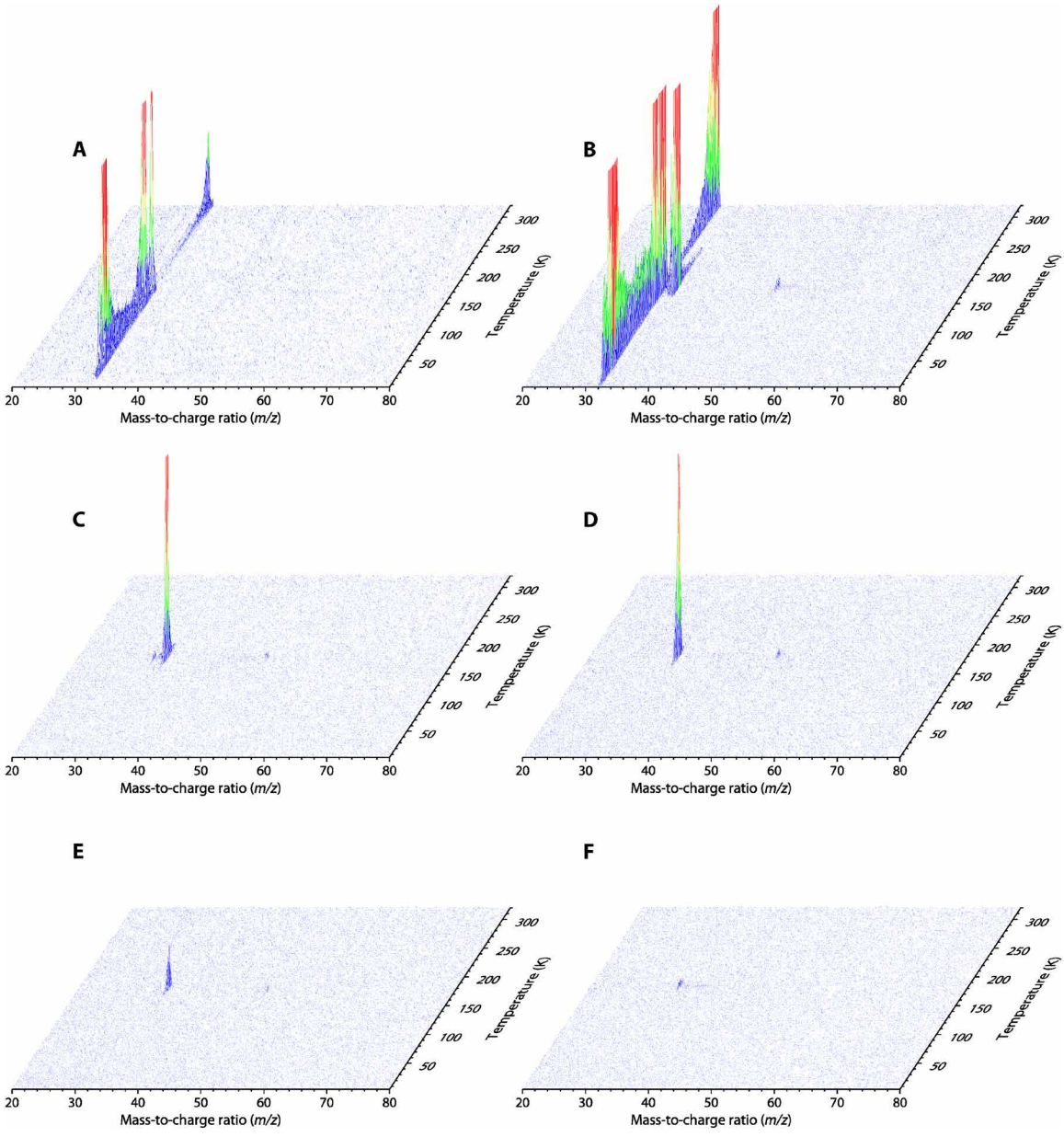

Fig. 2. SVUV-PI-ReTOF-MS at selected photon energies. SVUV-PI-ReTOF-MS data recorded during the TPD phase of nonirradiated H_2O-O_2 ice at the photon energy (PE) of (**A**) 12.20 eV (blank experiment) and irradiated H_2O-O_2 ice at PEs of (**B**) 12.20 eV, (**C**) 11.40 eV, (**D**) 11.30 eV, (**E**) 11.00 eV, and (**F**) 10.90 eV, respectively.

PIE curves

The PIE curves report the intensity of ion counts versus the photon energy at distinct *m*/*z*. For the irradiated H_2O-O_2 ices, the experimental PIE curves of photoionized products at *m*/*z* of 33 (HO_2^+), 34 ($H_2O_2^+$), and 50 ($H_2O_3^+$) were collected by scanning the photon energies from 10.80 to 12.20 eV in an interval of 0.10 eV (HO_2^+ and $H_2O_3^+$) and from 10.40 to 11.60 eV in an interval of 0.05 eV ($H_2O_2^+$), respectively, in the temperature range of 175 to 184 K (Fig. 4, A to C, and fig. S5). These PIE curves at *m*/*z* of 33, 34, and 50 display the onsets of ion counts at 11.35 ± 0.05 eV, 10.60 ± 0.03 eV, and 10.95 ± 0.05 eV, respectively.

The reported IE of 11.352 ± 0.007 eV for the hydroperoxyl radical HOO (*46*) matches well with the experimental onset of ion counts for *m*/*z* of 33 at 11.35 ± 0.05 eV, whereas the IE of HOOH of 10.631 ± 0.007 eV (*46*) correlates nicely with the onset of ion counts for *m*/*z* of 34 at 10.60 ± 0.03 eV. We emphasize that the appearance energy of HO_2^+ fragment from HOOH was determined to be 15.112 ± 0.035 eV (*46*), which cannot contribute to our experimental PIE curve recorded at *m*/*z* of 33. In addition, PIE curves collected in the present experiments at *m*/*z* of 33 and 34 agree exceptionally well with known literature PIE curves of HOO (*46*) and HOOH (*47*), respectively.

The onset of ion counts for *m*/*z* of 50 ($H_2O_3^+$) at 10.95 ± 0.05 eV is in line with the calculated IEs of *trans*-HOOOH (11.00 to 11.07 eV) and *cis*-HOOOH (10.90 to 10.97 eV), indicating the formation of *trans*-/*cis*-HOOOH, but not O(H_2O)O (11.09 to 11.16 eV). Nevertheless, no

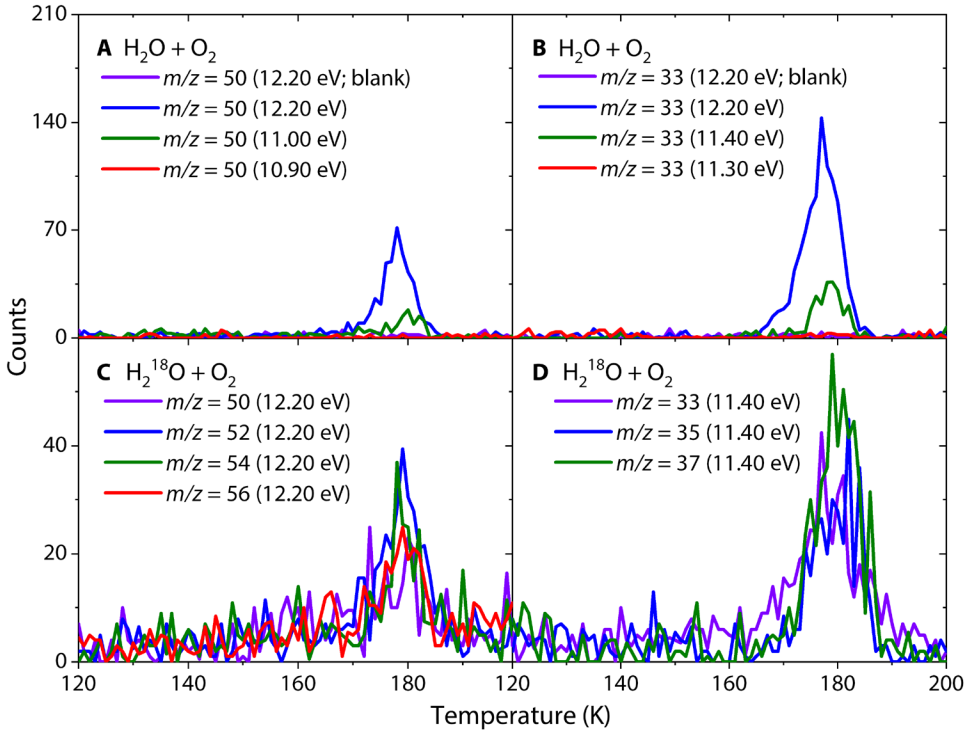

Fig. 3. TPD profiles. TPD profiles for (**A**) $m/z = 50$ of nonirradiated H_2O-O_2 ice at the PE of 12.20 eV (blank experiment) and irradiated H_2O-O_2 ices at PEs of 12.20, 11.00, and 10.90 eV, and (**B**) $m/z = 33$ of nonirradiated H_2O-O_2 ice at the PE of 12.20 eV and irradiated H_2O-O_2 ices at PEs of 12.20, 11.40, and 11.30 eV, respectively. TPD profiles obtained at (**C**) $m/z = 50$, 52, 54, and 56 at the PE of 12.20 eV and (**D**) $m/z = 33$, 35, and 37 at the PE of 11.40 eV of irradiated $H_2{}^{18}O$-O_2 ices.

reference PIE curve of any H_2O_3 isomer is available. Our computations in Franck-Condon factors (FCFs) from *trans*-/*cis*-HOOOH to the resulting cations including *trans*-*trans*-$HOOOH^+$, *cis*-*trans*-$HOOOH^+$, and *cis*-*cis*-$HOOOH^+$ (fig. S6) revealed that FCFs for the ionization from *trans*-HOOOH to *cis*-*cis*-$HOOOH^+$ are at least two orders of magnitude higher than the others. The computations correlate with the rapidly increasing PIE profile at an m/z of 50, which indicates an efficient adiabatic ionization at 10.95 ± 0.05 eV (Fig. 4C). This PIE curve then drops sharply in intensity beyond 11.25 ± 0.05 eV, suggesting an efficient dissociative ionization.

DISCUSSION

We further conducted an extensive computational search of entrance and exit channels leading to HOOOH on the global potential energy surface (PES) involving HOOOH neutrals and cations to elucidate the confirmative detection of HOOOH (Fig. 5). The computations predict that *cis*-*cis*-$HOOOH^+$ isomerizes promptly to the *cis*-*trans*-$HOOOH^+$, which undergoes unimolecular decomposition via a barrier of 1.09 eV to H_2O plus O_2^+ at the CCSD(T)/CBS//B3LYP/aug-cc-pVTZ + zero-point vibrational energy (ZPVE) level of theory. To account for potential multireference characters of this transition state, the dissociation barrier was further explored at the complete active-space second-order perturbation theory CASPT2(15,13)/def2-TZVP//B3LYP/aug-cc-pVTZ + ZPVE level of theory. At this level, the barrier turns out to be 11.30 eV and matches well the experimental PIE drop at 11.25 ± 0.05 eV for m/z of 50. In addition, this barrier also coincides with the appearance energy of 11.25 ± 0.05 eV in the dissociative channel of H_2O plus O_2^+ as indicated in the experimental PIE curve of O_2^+ (Fig. 4D and fig. S7). Notice that the ionization threshold of O_2 itself was measured to be 12.071 ± 0.001 eV (*48*).

We also carried out the comprehensive analysis of potential intersystem crossings (ISCs) in the reaction pathway involving the dissociative channel H_2O^+ plus $^3O_2$ (fig. S8). Starting from *cis*-*trans*-$HOOOH^+$, the CASPT2 energy scans showed that the energy on the doublet manifold increases, while the quartet state energy decreases as the HOO—OH bond stretches, resulting in the identification of the transition state TS4 at 11.54 eV. We located two minimum-energy crossing points MSX-1 and MSX-2 connecting to this transition state between the doublet and quartet surfaces, either of which can lead to the $H_2O^+\cdots{}^3O_2$ complex that dissociates barrierlessly to H_2O^+ plus $^3O_2$. This dissociative pathway could be responsible for the ionization onset of 11.55 ± 0.05 eV in the experimental PIE curve of H_2O^+ (Fig. 4D and fig. S7); this value is lower than the ionization threshold of H_2O located at 12.619 ± 0.006 eV (*49*). Alternative dissociative pathways of $HOOOH^+$ leading to H_2O^+ plus $^1O_2$, HO_2^+ plus OH, HO_3^+ plus H, and HO_2 plus OH^+ are located 12.32, 12.98, 14.44, and 16.87 eV higher than *trans*-HOOOH, respectively, and hence are closed energetically in our photoionization studies (tables S1 to S4). Overall, the agreement on the PIE curves and the ionization onsets of HOOOH along with the dissociative channels of H_2O plus O_2^+ and H_2O^+ plus $^3O_2$ between experiments and computations strongly supports the formation and detection of HOOOH molecules in our irradiated H_2O-O_2 ices.

Is it possible to detect HOOOH in deep space? Notably, HOO and HOOH—two coproducts of the interaction of ionizing radiation with H_2O-O_2 ices in the present experiments—have been detected

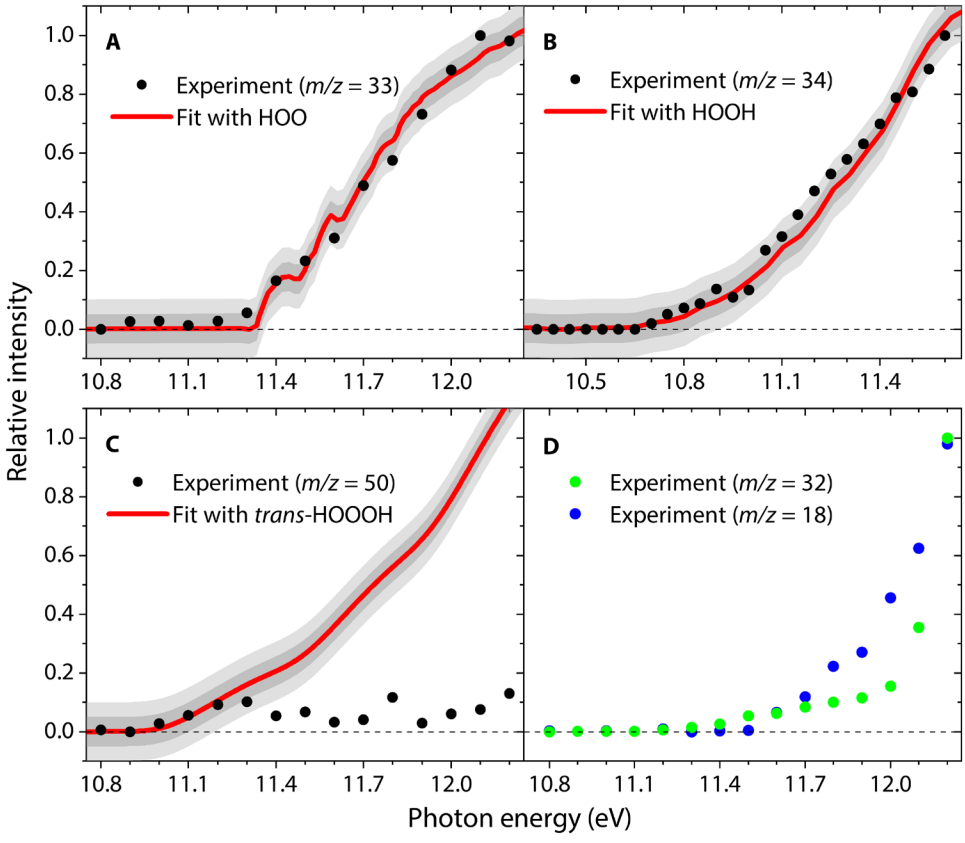

Fig. 4. PIE curves. PIE curves for the species linked to (**A**) $m/z = 33$, (**B**) $m/z = 34$, (**C**) $m/z = 50$, and (**D**) $m/z = 18$ and 32. The black, blue, and green dots represent the experimental data, while the red lines indicate the calculated or reference PIE curves. The experimental PIE curve at $m/z = 50$ drops at 11.25 ± 0.05 eV, while the experimental PIE curves at $m/z = 32$ and 18 rise at 11.25 ± 0.05 and 11.55 ± 0.05 eV, respectively. The uncertainties in the fit are noted with dark-gray (1σ) and light-gray (2σ) shaded regions.

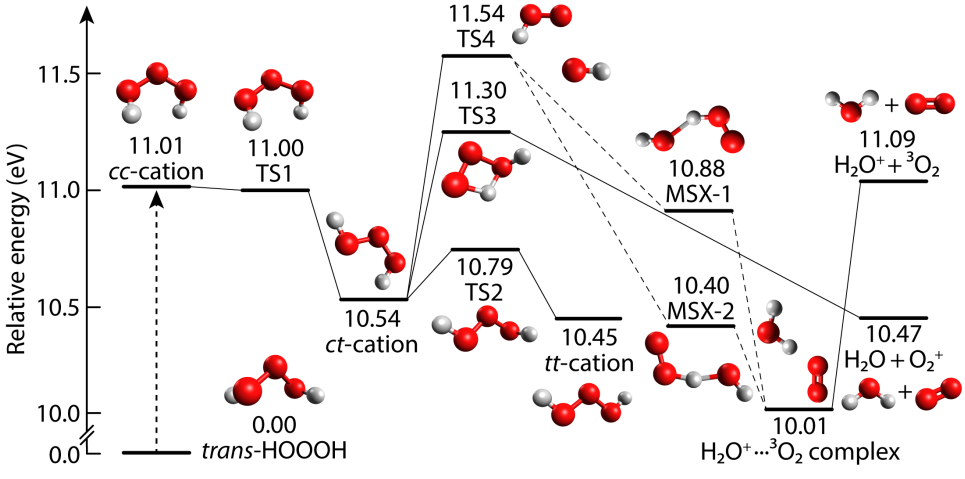

Fig. 5. The PES of the HOOOH neutral, cations, and dissociative channels. The *tt*-/*ct*-/*cc*-cation stands for the radical cations *trans-trans*-/*cis-trans*-/*cis-cis*-$HOOOH^+$, respectively. The dashed arrow indicates the adiabatic ionization process from *trans*-HOOOH to *cc*-cation, while the dashed lines connecting two minimum-energy crossing points (MSX-1 and MSX-2) represent the pathways involving the intersystem crossing (ISC). Atoms are color coded in white (hydrogen) and red (oxygen).

toward the cloud complex ρ Oph A (*50*, *51*). ρ Oph A also represents one of two interstellar clouds in which gas-phase O_2 was detected with abundance ratios of $HOO/O_2 \approx HOOH/O_2 \approx 0.6 \times 10^{-3}$ (*32*, *52*). Since both H_2O and O_2 are present toward ρ Oph A and the coproducts HOO and HOOH have been also detected, HOOOH should be existing after formation and sublimation from icy grains. On the other side, the abundance ratios of HOO and HOOH versus O_2 in the coma of comet 67P/Churyumov-Gerasimenko as determined by the Double Focusing Mass Spectrometer of the ROSINA instrument, are very close to those interstellar ones (*53*). The in situ measurement revealed local abundances of O_2 relative to H_2O ranging from 1 to 10%, suggesting that O_2 is chemically relevant to H_2O ice by radiolysis rather than CO_2 or CO ices (*35*). Therefore, astrophysical H_2O-O_2 ices under exposure of GCRs can be regarded as chemical and energetic sources in producing oxidizing agents including HOOOH, HOOH, HOO, and O_3 relevant to the extraterrestrial origin of life in deep space and the outer Solar System. The rotational frequency of *trans*-HOOOH (20838.6 MHz) (*21*) is potentially linked to the unidentified line (20838.2 MHz) observed in the W51 region (*54*), a massive molecular complex containing clusters of H_2O masers.

In conclusion, the present work provides compelling evidence for the identification of key oxidizing agents HOOOH, HOOH, HOO, and O_3 prepared in water–molecular oxygen (H_2O-O_2) ice analogs upon exposure to ionizing radiation in the form of proxies of GCRs. Although HOOOH has been studied extensively for more than one century, we demonstrate the formation and detection of HOOOH in interstellar and Solar System analog ices exploiting state-of-the-art SVUV-PI-ReTOF-MS, in association with high-level quantum chemical calculations, quadrupole mass spectrometry, and isotopic labeling experiments. The laboratory experiments conducted under conditions simulating astrophysical ones suggest that HOOOH can be produced in ices rich in H_2O and O_2 under the influence of ionizing radiation. The studies further suggest that HOOOH should be searched for and detected in the gas phase after sublimation from the icy grains toward ρ Oph A. The detection of interstellar HOOOH combined with updated astrochemical modeling would provide fundamental constraints and knowledge on the chemistry of oxygen-containing inorganic molecules in deep space. It would further provide a hitherto overlooked entry point to key oxidizers in prebiotic chemistry, eventually deciphering prebiotic redox cycles that could fuel microbial life on icy moons (*55*) or even oxygen-driven catalytic cycles such as the antibody catalysis in the oxidation of water (*56*).

MATERIALS AND METHODS

Experimental

The surface scattering experiments were conducted at the Shanghai-Hawaii-Hefei Advanced Research Center, using the VUV synchrotron radiation at the Combustion and Flame Beamline of the National Synchrotron Radiation Laboratory (NSRL) (*40*, *41*). The surface machine consists of a hydrogen-free stainless steel ultrahigh vacuum chamber that can be pumped down to a few 10^{-11} torr. The ice analogs were deposited onto a mirror-polished silver substrate (12.6×15.1 mm^2) attached to an oxygen-free high thermal conductivity copper coldfinger at 4.8 ± 0.1 K. High-purity H_2O (Macklin, high-performance liquid chromatography grade) and molecular O_2 (Air Liquide; 99.999%) were introduced and condensed onto the silver substrate via two sets of leak valves and glass capillary arrays (10-mm array diameter) at pressures of $(1 \pm 0.1) \times 10^{-8}$ and $(2 \pm 0.2) \times 10^{-8}$ torr, respectively, achieving an actual depositing ratio ($[H_2O]/[O_2]$) of 6.5 ± 1.0:1. This ratio was determined by an EI-QMS (Pfeiffer, QMG 220 M2). Before experiments using $H_2{}^{18}O$ (Aladdin; 97.0 atom % ^{18}O), tubings and chambers were purged with $H_2{}^{18}O$ vapor to allow any $^{16}O/^{18}O$ isotopic exchange to occur before the preparation of $H_2{}^{18}O$-O_2 ices. The thickness of deposited ices was measured via laser interferometry with a HeNe 632.8-nm laser (Thorlabs, HNL008L), which was determined to be 755 ± 50 nm based on analyzing the interference patterns and the average refractive index of the two components in amorphous ices, 1.26 ± 0.02 (Supplementary Methods and fig. S9) (*57*, *58*).

After deposition, the silver substrate was rotated and translated to the irradiation position and subjected to isothermal irradiation with 5-keV electrons (SPECS GmbH, EQ 22/35 electron source) at an incident angle of 70° relative to the surface normal. Distinct experiments were carried out under blank (0 nA for 60 min) and irradiated (1000 nA for 60 min, 1000 nA for 10 min, and 100 nA for 60 min) conditions (fig. S10). Using the CASINO 2.42 simulation software (*59*), the average penetration depth of the electrons (1000-nA current) was calculated to be 226 ± 23 nm (fig. S11), significantly less than the ice thickness, ensuring no interaction between the electrons and the silver substrate. The highest irradiation doses were calculated to be 99.2 eV per H_2O and 176.4 eV per O_2, respectively (table S5).

After irradiation, the ice sample was repositioned for TPD, annealing from 5 to 320 K at a rate of 1 K min^{-1} controlled and monitored by a programmable temperature controller (Lake Shore, Model 336) in an accuracy of ±0.1 K. Simultaneously, subliming molecules were mass analyzed via SVUV-PI-ReTOF-MS. Molecular ions at distinct *m*/*z* generated upon the selected photon energy were extracted by pulsed grid voltage (−150 V for 2.5 μs) and detected by a 40-mm dual-multichannel plate detector (Jordan TOF Products, C-726), whose signals were preamplified (AMETEK Inc., ORTEC 9306), discriminated and amplified (Advanced Research Instruments Corp., F-100TD), and recorded by a multichannel scaler (FAST ComTec, P7889) with 3.2-ns accuracy. Typical ReTOF mass spectra were generated at an experimental repetition rate of 15 kHz and a data acquisition time of 60 s, in accordance with the TPD rate. In the TPD range between 175 and 184 K, the SVUV photon energy was tuned from 10.80 to 12.20 eV in an interval of 0.10 eV or from 10.40 to 11.60 eV in an interval of 0.05 eV, to extract PIE curves of targeted molecules, which report the intensities of ions at specific *m*/*z* as a function of photon energy. During the SVUV photon energy scan, the obtained TPD spectra were normalized with respect to the TPD spectrum at 12.20 or 11.60 eV and the corresponding photon flux. Subliming molecules were also detected during TPD via the EI-QMS in the residual gas analyzer mode.

Computational

All density functional theory computations were carried out with Gaussian 16, Revision C.01 (*60*). For geometry optimizations and frequency computations, the B3LYP functional (*61*) was used with the Dunning correlation consistent split-valence basis set aug-cc-pVTZ (*62*). Vibrational frequency calculations were used to characterize stationary points and to obtain ZPVE corrections. Minimum structures were characterized by zero imaginary frequencies, while transition states exactly showed one imaginary frequency. On the basis of the minimum geometries, the corresponding frozen-core coupled cluster (*63*) CCSD(T)/aug-cc-pVTZ and CCSD(T)/aug-cc-pVQZ

single-point energies were computed and extrapolated to complete basis set limit (*64*) CCSD(T)/CBS using the built-in extrapolation routine in ORCA 5.0.4 (*65*). The adiabatic IEs were computed by taking the electronic CCSD(T)/CBS energies and the B3LYP/aug-cc-pVTZ ZPVE–corrected energy difference between the neutral and ionic species that correspond to similar conformations.

The analysis of ISCs between doublet and quartet states was carried out on a set of 49 smoothly transitioning structures along this pathway using Molpro (version 2025.1) (*66*, *67*). Calculations were performed using state-averaged complete active-space self-consistent field (*68*) wave functions, followed by CASPT2 (*69*–*71*) with the def2-TZVP basis set (*72*). The active space consisted of nine 2*p* orbitals from oxygen atoms and two 1*s* orbitals from hydrogen atoms. Two lowest doublet states and one lowest quartet state were considered to avoid root-flipping issues associated with nearly degenerate doublet states. A level shift of 0.3 was applied during CASPT2 calculations to prevent intruder state problems as recommended by Roos and Andersson (*73*).

Supplementary Materials

This PDF file includes:

Supplementary Methods
Figs. S1 to S11
Tables S1 to S5

REFERENCES AND NOTES

1. X. Xu, W. A. Goddard III, Peroxone chemistry: Formation of H_2O_3 and ring-$(HO_2)(HO_3)$ from O_3/H_2O_2. *Proc. Natl. Acad. Sci. U.S.A.* **99**, 15308–15312 (2002).
2. T. M. Lesko, A. Colussi, M. R. Hoffmann, Hydrogen isotope effects and mechanism of aqueous ozone and peroxone decompositions. *J. Am. Chem. Soc.* **126**, 4432–4436 (2004).
3. P. Wentworth Jr., J. E. McDunn, A. D. Wentworth, C. Takeuchi, J. Nieva, T. Jones, C. Bautista, J. M. Ruedi, A. Gutierrez, K. D. Janda, B. M. Babior, A. Eschenmoser, R. A. Lerner, Evidence for antibody-catalyzed ozone formation in bacterial killing and inflammation. *Science* **298**, 2195–2199 (2002).
4. D. Datta, N. Vaidehi, X. Xu, W. A. Goddard III, Mechanism for antibody catalysis of the oxidation of water by singlet dioxygen. *Proc. Natl. Acad. Sci. U.S.A.* **99**, 2636–2641 (2002).
5. J. Cerkovnik, B. Plesničar, Recent advances in the chemistry of hydrogen trioxide (HOOOH). *Chem. Rev.* **113**, 7930–7951 (2013).
6. M. Berthelot, Observations sur la décomposition du permanganate de potasse par l'eau oxygénée. *Compt. Rend.* **90**, 656 (1880). [Observations on the decomposition of potassium permanganate by hydrogen peroxide].
7. B. Plesničar, Progress in the chemistry of dihydrogen trioxide (HOOOH). *Acta Chim. Slov.* **52**, 1–12 (2005).
8. G. Czapski, B. H. Bielski, The formation and decay of H_2O_3 and HO_2 in electron-irradiated aqueous solutions. *J. Phys. Chem.* **67**, 2180–2184 (1963).
9. B. H. J. Bielski, H. A. Schwarz, Absorption spectra and kinetics of hydrogen sesquioxide and the perhydroxyl radical. *J. Phys. Chem.* **72**, 3836–3841 (1968).
10. B. H. J. Bielski, Kinetics of deuterium sesquioxide in heavy water. *J. Phys. Chem.* **74**, 3213–3216 (1970).
11. P. A. Giguère, K. Herman, Studies on hydrogen–oxygen systems in the electrical discharge. IV. Spectroscopic identification of the matrix-stabilized intermediates, H_2O_3 and H_2O_4. *Can. J. Chem.* **48**, 3473–3482 (1970).
12. P. A. Giguère, T. Srinivasan, Raman study of matrix isolated H_2O_2 and D_2O_2. *Chem. Phys. Lett.* **33**, 479–482 (1975).
13. J. Cerkovnik, B. Plesničar, Characterization and reactivity of hydrogen trioxide (HOOOH), a reactive intermediate formed in the low-temperature ozonation of 2-ethylanthrahydroquinone. *J. Am. Chem. Soc.* **115**, 12169–12170 (1993).
14. B. Plesničar, T. Tuttle, J. Cerkovnik, J. Koller, D. Cremer, Mechanism of formation of hydrogen trioxide (HOOOH) in the ozonation of 1,2-diphenylhydrazine and 1,2-dimethylhydrazine: An experimental and theoretical investigation. *J. Am. Chem. Soc.* **125**, 11553–11564 (2003).
15. B. Plesničar, J. Cerkovnik, J. Koller, F. Kovač, Chemistry of hydrotrioxides. Preparation, characterization, and reactivity of dimethylphenylsilyl hydrotrioxides. Hydrogen trioxide (HOOOH), a reactive intermediate in their thermal decomposition? *J. Am. Chem. Soc.* **113**, 4946–4953 (1991).
16. T. Tuttle, J. Cerkovnik, B. Plesničar, D. Cremer, Hemiortho esters and hydrotrioxides as the primary products in the low-temperature ozonation of cyclic acetals: An experimental and theoretical investigation. *J. Am. Chem. Soc.* **126**, 16093–16104 (2004).
17. J. Koller, B. Plesničar, Mechanism of the participation of water in the decomposition of hydrogen trioxide (HOOOH). A theoretical study. *J. Am. Chem. Soc.* **118**, 2470–2472 (1996).
18. X. Zhu, P. Wentworth Jr., A. D. Wentworth, A. Eschenmoser, R. A. Lerner, I. A. Wilson, Probing the antibody-catalyzed water-oxidation pathway at atomic resolution. *Proc. Natl. Acad. Sci. U.S.A.* **101**, 2247–2252 (2004).
19. A. Engdahl, B. Nelander, The vibrational spectrum of H_2O_3. *Science* **295**, 482–483 (2002).
20. X. Xu, R. P. Muller, W. A. Goddard III, The gas phase reaction of singlet dioxygen with water: A water-catalyzed mechanism. *Proc. Natl. Acad. Sci. U.S.A.* **99**, 3376–3381 (2002).
21. K. Suma, Y. Sumiyoshi, Y. Endo, The rotational spectrum and structure of HOOOH. *J. Am. Chem. Soc.* **127**, 14998–14999 (2005).
22. D. S. Hollman, H. F. Schaefer, In search of the next holy grail of polyoxide chemistry: Explicitly correlated ab initio full quartic force fields for HOOH, HOOOH, HOOOOH, and their isotopologues. *J. Chem. Phys.* **136**, 084302 (2012).
23. E. F. Van Dishoeck, E. Herbst, D. A. Neufeld, Interstellar water chemistry: From laboratory to observations. *Chem. Rev.* **113**, 9043–9085 (2013).
24. K. Murakawa, M. Tamura, T. Nagata, 1-4 micron spectrophotometry of dust in the Taurus dark cloud: Water ice distribution in Heiles cloud 2. *Astrophys. J. Suppl. Ser.* **128**, 603 (2000).
25. D. C. Jewitt, J. Luu, Crystalline water ice on the Kuiper belt object (50000) Quaoar. *Nature* **432**, 731–733 (2004).
26. M. E. Brown, The compositions of Kuiper belt objects. *Annu. Rev. Earth Planet. Sci.* **40**, 467–494 (2012).
27. G. Filacchione, M. C. De Sanctis, F. Capaccioni, A. Raponi, F. Tosi, M. Ciarniello, P. Cerroni, G. Piccioni, M. Capria, E. Palomba, Exposed water ice on the nucleus of comet 67P/Churyumov–Gerasimenko. *Nature* **529**, 368–372 (2016).
28. M. C. De Sanctis, F. Capaccioni, M. Ciarniello, G. Filacchione, M. Formisano, S. Mottola, A. Raponi, F. Tosi, D. Bockelée-Morvan, S. Erard, The diurnal cycle of water ice on comet 67P/Churyumov–Gerasimenko. *Nature* **525**, 500–503 (2015).
29. R. H. Brown, D. P. Cruikshank, Determination of the composition and state of icy surfaces in the outer solar system. *Annu. Rev. Earth Planet. Sci.* **25**, 243–277 (1997).
30. S. R. Taylor, *Solar System Evolution: A New Perspective* (Cambridge Univ. Press, 2001).
31. P. F. Goldsmith, R. Liseau, T. A. Bell, J. H. Black, J.-H. Chen, D. Hollenbach, M. J. Kaufman, D. Li, D. C. Lis, G. Melnick, Herschel measurements of molecular oxygen in Orion. *Astrophys. J.* **737**, 96 (2011).
32. R. Liseau, P. Goldsmith, B. Larsson, L. Pagani, P. Bergman, J. Le Bourlot, T. Bell, A. Benz, E. Bergin, P. Bjerkeli, Multi-line detection of O_2 toward ρ Ophiuchi A. *Astron. Astrophys.* **541**, A73 (2012).
33. W. M. Calvin, R. N. Clark, R. H. Brown, J. R. Spencer, Spectra of the icy Galilean satellites from 0.2 to 5μm: A compilation, new observations, and a recent summary. *J. Geophys. Res.* **100**, 19041–19048 (1995).
34. J. R. Spencer, W. M. Calvin, Condensed O_2 on Europa and Callisto. *Astrophys. J.* **124**, 3400–3403 (2002).
35. A. Luspay-Kuti, O. Mousis, F. Pauzat, O. Ozgurel, Y. Ellinger, J. I. Lunine, S. A. Fuselier, K. E. Mandt, K. J. Trattner, S. M. Petrinec, Dual storage and release of molecular oxygen in comet 67P/Churyumov–Gerasimenko. *Nat. Astron.* **6**, 724–730 (2022).
36. M. Moore, R. Hudson, IR detection of H_2O_2 at 80 K in ion-irradiated laboratory ices relevant to Europa. *Icarus* **145**, 282–288 (2000).
37. P. D. Cooper, M. H. Moore, R. L. Hudson, Infrared detection of HO_2 and HO_3 radicals in water ice. *J. Phys. Chem. A* **110**, 7985–7988 (2006).
38. P. D. Cooper, M. H. Moore, R. L. Hudson, Radiation chemistry of H_2O+O_2 ices. *Icarus* **194**, 379–388 (2008).
39. W. Zheng, D. Jewitt, R. I. Kaiser, Mechanistical studies on the formation of isotopomers of hydrogen peroxide (HOOH), hydrotrioxy (HOOO), and dihydrogentrioxide (HOOOH) in electron-irradiated $H_2{}^{18}O/O_2$ ice mixtures. *Phys. Chem. Chem. Phys.* **9**, 2556–2563 (2007).
40. C. Zhu, H. Wang, I. Medvedkov, J. Marks, M. Xu, J. Yang, T. Yang, Y. Pan, R. I. Kaiser, Exploitation of synchrotron radiation photoionization mass spectrometry in the analysis of complex organics in interstellar model ices. *J. Phys. Chem. Lett.* **13**, 6875–6882 (2022).
41. J. H. Marks, X. Bai, A. A. Nikolayev, Q. a. Gong, C. Zhu, N. F. Kleimeier, A. M. Turner, S. K. Singh, J. Wang, J. Yang, Methanetriol—Formation of an impossible molecule. *J. Am. Chem. Soc.* **146**, 12174–12184 (2024).
42. J. Wang, J. H. Marks, R. C. Fortenberry, R. I. Kaiser, Interstellar formation of glyceric acid $[HOCH_2CH(OH)COOH]$—The simplest sugar acid. *Sci. Adv.* **10**, eadl3236 (2024).
43. C. Zhu, R. Frigge, A. Bergantini, R. C. Fortenberry, R. I. Kaiser, Untangling the formation of methoxymethanol (CH_3OCH_2OH) and dimethyl peroxide (CH_3OOCH_3) in star-forming regions. *Astrophys. J.* **881**, 156 (2019).
44. P. A. Denis, F. R. Ornellas, Theoretical characterization of hydrogen polyoxides: HOOH, HOOOH, HOOOOH, and HOOO. *J. Phys. Chem. A* **113**, 499–506 (2009).
45. L. Wang, W. Wu, J. Zhang, Z. Cao, Theoretical study on the electronic spectra of *cis*-HOOOH and *trans*-HOOOH. *Acta Phys. Chim. Sin.* **22**, 1079–1084 (2006).

46. M. Litorja, B. Ruscic, A photoionization study of the hydroperoxyl radical, HO_2, and hydrogen peroxide, H_2O_2. *J. Electron. Spectrosc. Relat. Phenom.* **97**, 131–146 (1998).
47. B. Dong, Z. Hu, Q. Xu, B. Liu, Q. Zhu, J. Guan, C. Liu, Y. Pan, L. Hu, J. Fang, Improving quantification of hydrogen peroxide by synchrotron vacuum ultraviolet photoionization mass spectrometry. *Combust. Flame* **242**, 112214 (2022).
48. J. A. Samson, J. Gardner, On the ionization potential of molecular oxygen. *Can. J. Phys.* **53**, 1948–1952 (1975).
49. D. Katayama, R. Huffman, C. O'Bryan, Absorption and photoionization cross sections for H_2O and D_2O in the vacuum ultraviolet. *J. Chem. Phys.* **59**, 4309–4319 (1973).
50. P. Bergman, B. Parise, R. Liseau, B. Larsson, H. Olofsson, K. Menten, R. Güsten, Detection of interstellar hydrogen peroxide. *Astron. Astrophys.* **531**, L8 (2011).
51. B. Parise, P. Bergman, F. Du, Detection of the hydroperoxyl radical HO_2 toward ρ Ophiuchi A. *Astron. Astrophys.* **541**, L11 (2012).
52. B. Larsson, R. Liseau, L. Pagani, P. Bergman, P. Bernath, N. Biver, J. H. Black, R. Booth, V. Buat, J. Crovisier, Molecular oxygen in the ρ Ophiuchi cloud. *Astron. Astrophys.* **466**, 999–1003 (2007).
53. A. Bieler, K. Altwegg, H. Balsiger, A. Bar-Nun, J.-J. Berthelier, P. Bochsler, C. Briois, U. Calmonte, M. Combi, J. De Keyser, Abundant molecular oxygen in the coma of comet 67P/Churyumov–Gerasimenko. *Nature* **526**, 678–681 (2015).
54. M. Bell, L. Avery, J. Watson, A spectral-line survey of W51 from 17.6 to 22.0 GHz. *Astrophys. J. Suppl. Ser.* **86**, 211–233 (1993).
55. C. F. Chyba, Energy for microbial life on Europa. *Nature* **403**, 381–382 (2000).
56. P. Wentworth Jr., L. H. Jones, A. D. Wentworth, X. Zhu, N. A. Larsen, I. A. Wilson, X. Xu, W. A. Goddard III, K. D. Janda, A. Eschenmoser, Antibody catalysis of the oxidation of water. *Science* **293**, 1806–1811 (2001).
57. J. Elsila, L. J. Allamandola, S. A. Sandford, The 2140 cm^{-1} (4.673 microns) solid CO band: The case for interstellar O_2 and N_2 and the photochemistry of nonpolar interstellar ice analogs. *Astrophys. J.* **479**, 818–838 (1997).
58. M. Bouilloud, N. Fray, Y. Benilan, H. Cottin, M. C. Gazeau, A. Jolly, Bibliographic review and new measurements of the infrared band strengths of pure molecules at 25 K: H_2O, CO_2, CO, CH_4, NH_3, CH_3OH, HCOOH and H_2CO. *Mon. Not. R. Astron. Soc.* **451**, 2145–2160 (2015).
59. D. Drouin, A. R. Couture, D. Joly, X. Tastet, V. Aimez, R. Gauvin, CASINO V2.42: A fast and easy-to-use modeling tool for scanning electron microscopy and microanalysis users. *Scanning* **29**, 92–101 (2007).
60. M. J. Frisch, G. W. Trucks, H. B. Schlegel, G. E. Scuseria, M. A. Robb, J. R. Cheeseman, G. Scalmani, V. Barone, G. A. Petersson, H. Nakatsuji, X. Li, M. Caricato, A. V. Marenich, J. Bloino, B. G. Janesko, R. Gomperts, B. Mennucci, H. P. Hratchian, J. V. Ortiz, A. F. Izmaylov, J. L. Sonnenberg, Williams, F. Ding, F. Lipparini, F. Egidi, J. Goings, B. Peng, A. Petrone, T. Henderson, D. Ranasinghe, V. G. Zakrzewski, J. Gao, N. Rega, G. Zheng, W. Liang, M. Hada, M. Ehara, K. Toyota, R. Fukuda, J. Hasegawa, M. Ishida, T. Nakajima, Y. Honda, O. Kitao, H. Nakai, T. Vreven, K. Throssell, J. A. Montgomery Jr., J. E. Peralta, F. Ogliaro, M. J. Bearpark, J. J. Heyd, E. N. Brothers, K. N. Kudin, V. N. Staroverov, T. A. Keith, R. Kobayashi, J. Normand, K. Raghavachari, A. P. Rendell, J. C. Burant, S. S. Iyengar, J. Tomasi, M. Cossi, J. M. Millam, M. Klene, C. Adamo, R. Cammi, J. W. Ochterski, R. L. Martin, K. Morokuma, O. Farkas, J. B. Foresman, D. J. Fox, Revision C.01, Gaussian, Inc. (Gaussian Inc., Wallingford, CT, 2016).
61. A. D. Becke, Density-functional thermochemistry. III. The role of exact exchange. *J. Chem. Phys.* **98**, 5648–5652 (1993).
62. R. A. Kendall, T. H. Dunning, R. J. Harrison, Electron affinities of the first-row atoms revisited. Systematic basis sets and wave functions. *J. Chem. Phys.* **96**, 6796–6806 (1992).
63. J. F. Stanton, Why CCSD(T) works: A different perspective. *Chem. Phys. Lett.* **281**, 130–134 (1997).
64. K. A. Peterson, D. E. Woon, T. H. Dunning, Benchmark calculations with correlated molecular wave functions. IV. The classical barrier height of the $H+H_2 \rightarrow H_2+H$ reaction. *J. Chem. Phys.* **100**, 7410–7415 (1994).
65. F. Neese, Software update: The ORCA program system, version 4.0. *WIRES Comput. Mol. Sci.* **8**, e1327 (2018).
66. H. J. Werner, P. J. Knowles, G. Knizia, F. R. Manby, M. Schütz, Molpro: A general-purpose quantum chemistry program package. *Wiley Interdiscip. Rev. Comput. Mol. Sci.* **2**, 242–253 (2012).
67. H.-J. Werner, P. J. Knowles, F. R. Manby, J. A. Black, K. Doll, A. Heßelmann, D. Kats, A. Köhn, T. Korona, D. A. Kreplin, The Molpro quantum chemistry package. *J. Chem. Phys.* **152**, 144107 (2020).
68. B. O. Roos, P. R. Taylor, P. E. Sigbahn, A complete active space SCF method (CASSCF) using a density matrix formulated super-CI approach. *Chem. Phys.* **48**, 157–173 (1980).
69. P. Celani, H.-J. Werner, Multireference perturbation theory for large restricted and selected active space reference wave functions. *J. Chem. Phys.* **112**, 5546–5557 (2000).
70. T. Shiozaki, W. Győrffy, P. Celani, H.-J. Werner, Communication: Extended multi-state complete active space second-order perturbation theory: Energy and nuclear gradients. *J. Chem. Phys.* **135**, 081106 (2011).
71. W. Győrffy, T. Shiozaki, G. Knizia, H.-J. Werner, Analytical energy gradients for second-order multireference perturbation theory using density fitting. *J. Chem. Phys.* **138**, 104104 (2013).
72. F. Weigend, R. Ahlrichs, Balanced basis sets of split valence, triple zeta valence and quadruple zeta valence quality for H to Rn: Design and assessment of accuracy. *Phys. Chem. Chem. Phys.* **7**, 3297–3305 (2005).
73. B. O. Roos, K. Andersson, Multiconfigurational perturbation theory with level shift—The Cr_2 potential revisited. *Chem. Phys. Lett.* **245**, 215–223 (1995).

Acknowledgments: We thank the Information Technology Services (ITS) from the University of Hawaii at Manoa for the computational resources. **Funding:** This work was conducted under a Memorandum of Understanding (MOU) between the East China Normal University (ECNU), the University of Hawaii at Manoa (UHM), and the National Synchrotron Radiation Laboratory (NSRL). Z.S. and T.Y. thank the support from the National Natural Science Foundation of China (grants nos. 12034008, 12250003, and 92461301). T.Y. thanks the National Natural Science Foundation of China (grant no. 12274140), the Xinjiang Tianchi Talent Program (2023), the Program for Professor of Special Appointment (Eastern Scholar) at the Shanghai Institutions of Higher Learning, the Young Top-Notch Talent Support Program of Shanghai, and the Natural Science Foundation of Shanghai (grant no. 22ZR1421400) for funding. R.I.K. thanks the National Science Foundation for support (NSF AST 2403867). A.K.E. thanks the Fonds der Chemischen Industrie and the Deutsche Forschungsgemeinschaft (DFG; German Research Foundation) under Germany's Excellence Strategy—EXC-2033–390677874 – RESOLV—for funding. **Author contributions:** Conceptualization: T.Y. and R.I.K. Methodology: T.Y., R.I.K., and Z.S. Software: C.L., Y.L., A.K.E., and R.S. Validation: X.B., C.L., A.K.E., R.S., R.I.K., and T.Y. Formal analysis: X.B., Y.L., and A.K.E. Investigation: X.B., C.L., Y.L., Q.G., J.L., J.Y., Y.P., and Z.S. Resources: J.Y., Y.P., Z.S., A.K.E., R.S., R.I.K., and T.Y. Data curation: Q.G. Writing—original draft: X.B. and T.Y. Writing—review and editing: X.B., Y.L., Z.S., A.K.E., R.S., R.I.K., and T.Y. Visualization: X.B., C.L., Y.L., and A.K.E. Supervision: X.B., Y.P., A.K.E., R.S., Z.S., R.I.K., and T.Y. Project administration: X.B., Y.P., A.K.E., R.S., R.I.K., T.Y. Funding acquisition: Z.S., A.K.E., R.S., R.I.K., and T.Y. **Competing interests:** The authors declare they have no competing interests. **Data and materials availability:** All data needed to evaluate the conclusions in the paper are present in the paper and/or the Supplementary Materials.

Submitted 8 February 2025
Accepted 17 July 2025
Published 15 August 2025
10.1126/sciadv.adw5720